

Numerical Simulations of Snake Dissipative Solitons in Complex Cubic-Quintic Ginzburg-Landau Equation

Stefan C. Mancas
and

Harihar Khanal
Embry-Riddle Aeronautical University, Daytona Beach, USA
mancass@erau.edu
khana66a@erau.edu

Numerical simulations of the complex cubic-quintic Ginzburg-Landau equation (CCQGLE), a canonical equation governing the weakly nonlinear behavior of dissipative systems in a wide variety of disciplines, reveal five entirely novel classes of pulse or solitary waves solutions, viz. pulsating, creeping, snaking, erupting, and chaotical solitons [9]. Here, we develop a theoretical framework for analyzing the full spatio-temporal structure of one class of dissipative solution (snaking soliton) of the CCQGLE using the variational approximation technique and the dynamical systems theory. The qualitative behavior of the snaking soliton is investigated using the numerical simulations of (a) the full nonlinear complex partial differential equation and (b) a system of three ordinary differential equations resulting from the variational approximation.

I. INTRODUCTION

The complex cubic-quintic Ginzburg-Landau equation (CCQGLE) is one of the most widely studied nonlinear equations. In fluid mechanics, it is also often referred to as the Newell-Whitehead equation after the authors who derived it in the context of Bénard convection. Many basic properties of the equation and its solutions are reviewed in [2], together with applications to a vast variety of phenomena including nonlinear waves, second-order phase transitions, superconductivity, superfluidity, Bose-Einstein condensation, liquid crystals and string theory.

Due to the highly nonlinear nature of the CCQGLE, analytic solutions have been limited to special cases. Thus, its numerical approximations have become valuable tools in order to better understand the theoretical insight into the problem. Numerical simulations in [9] identify five entirely novel classes of pulse or solitary waves solutions, viz. pulsating, creeping, snaking, erupting, and chaotical solitons of the CCQGLE. In contrast to the regular solitary waves investigated in numerous integrable and non-integrable systems over the last three decades, these dissipative solitons are not stationary in time. Rather, they are spatially confined pulse-type structures whose envelopes exhibit complicated temporal dynamics.

In this paper we describe a theoretical framework for analyzing the full spatiotemporal structure of one class of solitary waves (snaking soliton) of the CCQGLE, and present numerical simulations resulting from the full nonlinear partial differential equation, as well as systems of ODEs from the variational approximation technique.

First, we develop and discuss a variational formalism within which to explore the various classes of dissipative solitons. We find a suitable Lagrangian based on ansatz. Then the resulting Euler-Lagrange equations are treated in a completely novel way. Rather than considering on the stable fixed points which correspond to the well-known stationary solitons or plain pulses, we use dynamical systems theory to focus on more complex attractors viz. periodic, quasiperiodic, and chaotic ones. Periodic evolution of the trial function parameters on a stable periodic attractor would yield solitons whose amplitudes are non-stationary or time dependent. In particular, pulsating, snaking (and less easily, creeping) dissipative solitons may be treated using stable periodic attractors of various trial function parameters. Chaotic evolution of the trial function parameters would yield to chaotic solitary waves. In the language of the Los Alamos school, the fully spatiotemporal approach followed here may be said to be the “collective coordinates” formulation. In other words, we consider a pulse or solitary wave at any time as a coherent collective entity (or coordinate). This solitary wave is then temporally modulated. The spatial approach proposed, and explored, in this paper is the variational method. However, the method is very significantly and non-trivially generalized from all earlier applications to deal with our novel classes of dissipative solitary waves.

Next, we solve (a) the initial boundary value problem of the CCQGLE and (b) the initial value problem of the Euler-Lagrange system resulting from the variational approximation numerically. The numerical scheme

for the PDE is based on a Finite Difference discretization of the partial differential equation with a low storage variant explicit Runge-Kutta third order method. The Euler-Lagrange system of ODEs is solved numerically using the MATLAB's built-in function `ode45`.

The remainder of this paper is organized as follows. Section §2 describes briefly the CCQGLE as well as the classes of its soliton solutions. An ODE system resulting from the generalized variational formulation of the CCQGLE and Hopf bifurcation theory are also presented here. In section §3 numerical methods for the IVP and BVP are discussed. Sections §4 and §5 deal with the simulation results from previous section using the PDE and the variational formulation. Finally, in section §5 we summarize the results and conclude the paper outlining some further research directions.

II. DESCRIPTION OF CCQGLE

An important element in the long time dynamics of pattern forming systems is a class of solutions which we call “coherent structures” or solitons. These structure could be a profile of light intensity, temperature, magnetic field, etc. A dissipative soliton is localized and exists for an extended period of time. Its parts are experiencing gain/loss of energy or mass with the medium. Thus, energy and matter can flow into the system through its boundaries. As long as the parameters in the system stay constant, the structure that could evolve by changing shape exists indefinitely in time. The structure disappears when the source is switched off, or if the parameters are moved outside the range of existence of the soliton solutions. Since these dissipative systems include energy exchange with external sources, they are no longer Hamiltonian, and the solitons solutions in these systems are also qualitatively different from those in Hamiltonian systems. In Hamiltonian systems, soliton solutions appear as a result of balance between diffraction (dispersion) and nonlinearity. Diffraction spreads a beam while nonlinearity will focus it and make it narrower. The balance between the two results in stationary solitary wave solutions, which usually form a one parameter family. In dissipative systems with gain and loss, in order to have stationary solutions, the gain and loss must be also balanced. This additional balance results in solutions which are fixed. Then the shape, amplitude and the width are all completely fixed by the parameters of the dissipative equation. However, the solitons, when they exist, can again be considered as “modes” of dissipative systems just as for non-dissipative ones.

Recent perturbative treatments based on expressions about the nonlinear Schrödinger equations are generalized to perturbations of the cubic-quintic and derivative Schrödinger equations. The cubic Ginzburg-Landau admits a selected range of exact soliton solutions [7]. These exist when certain relations between parameters are satisfied. However, this certainly does not imply that the equations are integrable. Dissipative systems, as it is the case with Burger's equation are integrable. In reality, general dissipative nonlinear PDEs cannot be reduced to linear equations in any known way, therefore an insight to the type of solutions that the equation has may be based on numerical simulations.

The simplest mode that can account for this type of behavior is the Ginzburg-Landau model, with the corresponding cubic-quintic equations in the form [13]

$$\partial_t A = \epsilon A + (b_1 + ic_1)\partial_x^2 A - (b_3 - ic_3)|A|^2 A - (b_5 - ic_5)|A|^4 A. \quad (\text{II.1})$$

The present study will confine itself to spatially infinite systems in one dimension and will focus primarily on a spatio-temporal behavior of dissipative solitons. One way to approach this problem and to arrive at (II.1) is to start with the well known modified Schrödinger equation

$$\partial_t A = ic_1 \partial_x^2 A + ic_3 |A|^2 A + ic_5 |A|^4 A + \partial_x [(s_0 + s_2 |A|^2) A], \quad (\text{II.2})$$

and to perturb with a dissipative term [6] in special parameter regimes, with terms on the rhs. of (II.2) of the form $f(A) = \epsilon A + b_1 \partial_x^2 A - b_3 |A|^2 A - b_5 |A|^4 A$.

The unperturbed system (II.2) leads to an integrable dynamical system whose orbits can be calculated analytically [4].

The interpretation of the system's parameters in (II.1) depends on the particular field of work. For example, in optics, t is the propagation distance or the cavity number, x is the transverse variable, the angular spectral gain or loss is identified by b_1 , c_1 is the second-order diffraction or linear dispersion, b_3 is the nonlinear gain or 2-photon absorption if negative, c_3 is the nonlinear dispersion, ϵ is the difference between linear gain and loss, b_5 represents the saturation of the nonlinear gain, and c_5 the saturation of the nonlinear refractive index. In physical problems, the quintic nonlinearity is even of higher importance than the cubic one, as it is responsible for stability of localized solutions.

A special case of (II.1) is the nonlinear Schrödinger equation ($\epsilon = b_1 = b_3 = b_5 = c_5 = 0, c_1 = 1$) 3

$$\partial_t A = i\partial_x^2 A + ic_3|A|^2 A \quad (\text{II.3})$$

which is both Hamiltonian and integrable. Its extension, the quintic-cubic Schrödinger equation ($\epsilon = b_1 = b_3 = b_5 = 0, c_1 = 1$)

$$\partial_t A = i\partial_x^2 A + ic_3|A|^2 A + ic_5|A|^4 A \quad (\text{II.4})$$

is Hamiltonian but non-integrable. Other interesting cases are the derivative nonlinear Schrödinger equation

$$\partial_t A = i\partial_x^2 A + s_0\partial_x A + s_2\partial_x(|A|^2 A) \quad (\text{II.5})$$

and the combinations of last two, which is the quintic derivative Schrödinger equation

$$\partial_t A = i\partial_x^2 A + s_0\partial_x A + s_2\partial_x(|A|^2 A) + ic_3|A|^2 A + ic_5|A|^4 A. \quad (\text{II.6})$$

A. Euler-Lagrange Equations

Employing the generalized variational formulations and proceeding as in [8], the Lagrangian for the CC-QGLE (II.1) may be written as [10]

$$\begin{aligned} \mathcal{L} = r^* & [\partial_t A - \epsilon A - (b_1 + ic_1)\partial_x^2 A + (b_3 - ic_3)|A|^2 A + (b_5 - ic_5)|A|^4 A] \\ & + r [\partial_t A^* - \epsilon A^* - (b_1 - ic_1)\partial_x^2 A^* + (b_3 + ic_3)|A|^2 A^* + (b_5 + ic_5)|A|^4 A^*]. \end{aligned} \quad (\text{II.7})$$

Here r is the usual auxiliary equation employed in [8] and it satisfies a perturbative evolution equation dual to the CCQGLE with all non-Hamiltonian terms reversed in sign. Choosing the single-humped trial functions of the form:

$$A(x, t) = A_1(t)e^{-\sigma_1(t)^2[x-\phi_1(t)]^2} e^{i\alpha_1(t)} e^{i\psi(t)^2 x^2} \quad (\text{II.8})$$

$$r(x, t) = e^{-\sigma_2(t)^2[x-\phi_2(t)]^2} e^{i\alpha_2(t)} \quad (\text{II.9})$$

where the $A_1(t)$ is the amplitude, the $\sigma_i(t)$'s are the inverse widths, $\phi_i(t)$'s are the positions (with $\dot{\phi}_i(t)$ the speed), $e^{i\psi(t)^2 x^2}$ represents the chirp, $\alpha_i(t)$'s are the phases of the solitons and are all allowed to vary arbitrarily in time. For now, the chirp terms are omitted for simplicity. Substituting (II.8)/(II.9) in (II.7)

$$\begin{aligned}
L_{EFF} = \int_{-\infty}^{\infty} \mathcal{L} dx = 2\sqrt{\pi} \left\{ & - \frac{e^{-\frac{\sigma_1(t)^2 \sigma_2(t)^2 [\phi_1(t) - \phi_2(t)]^2}{\sigma_1(t)^2 + \sigma_2(t)^2}}}{[\sigma_1(t)^2 + \sigma_2(t)^2]^{\frac{1}{2}}} \epsilon A_1(t) \cos[\alpha_1(t) - \alpha_2(t)] \right. \\
& + \frac{e^{-\frac{3\sigma_1(t)^2 \sigma_2(t)^2 [\phi_1(t) - \phi_2(t)]^2}{3\sigma_1(t)^2 + \sigma_2(t)^2}}}{[3\sigma_1(t)^2 + \sigma_2(t)^2]^{\frac{1}{2}}} A_1(t)^3 \left[b_3 \cos[\alpha_1(t) - \alpha_2(t)] + c_3 \sin[\alpha_1(t) - \alpha_2(t)] \right] \\
& + \frac{e^{-\frac{5\sigma_1(t)^2 \sigma_2(t)^2 [\phi_1(t) - \phi_2(t)]^2}{5\sigma_1(t)^2 + \sigma_2(t)^2}}}{[5\sigma_1(t)^2 + \sigma_2(t)^2]^{\frac{1}{2}}} A_1(t)^5 \left[b_5 \cos[\alpha_1(t) - \alpha_2(t)] + c_5 \sin[\alpha_1(t) - \alpha_2(t)] \right] \\
& + \frac{e^{-\frac{\sigma_1(t)^2 \sigma_2(t)^2 [\phi_1(t) - \phi_2(t)]^2}{\sigma_1(t)^2 + \sigma_2(t)^2}}}{[\sigma_1(t)^2 + \sigma_2(t)^2]^{\frac{5}{2}}} \left[\cos[\alpha_1(t) - \alpha_2(t)] [\sigma_1(t)^2 + \sigma_2(t)^2]^2 \dot{A}_1(t) \right. \\
& + A_1(t) \left(-2\sigma_1(t)^2 \sigma_2(t)^2 [b_1 \cos[\alpha_1(t) - \alpha_2(t)] - c_1 \sin[\alpha_1(t) - \alpha_2(t)]] [-\sigma_2(t)^2 \right. \\
& + \sigma_1(t)^2 [-1 + 2\sigma_2(t)^2 [\phi_1(t) - \phi_2(t)]^2] - \dot{\alpha}_1(t) \sin[\alpha_1(t) - \alpha_2(t)] [\sigma_1(t)^2 + \sigma_2(t)^2]^2 \\
& - \sigma_1(t) \dot{\sigma}_1(t) \cos[\alpha_1(t) - \alpha_2(t)] [\sigma_1(t)^2 + \sigma_2(t)^2 + 2\sigma_2(t)^4 [\phi_1(t) - \phi_2(t)]^2] \\
& \left. \left. \left. - 2\dot{\phi}_1(t) \sigma_1(t)^2 \sigma_2(t)^2 [\phi_1(t) - \phi_2(t)] [\sigma_1(t)^2 + \sigma_2(t)^2] \cos[\alpha_1(t) - \alpha_2(t)] \right) \right] \right\}. \tag{II.10}
\end{aligned}$$

Since (II.10) reveals that only the relative phase $\alpha(t) = \alpha_1(t) - \alpha_2(t)$, and relative velocity $\phi(t) = \phi_1(t) - \phi_2(t)$ of $A(x, t)$ and $r(x, t)$ are relevant, we henceforth rescale them according to

$$\alpha_1(t) = \alpha(t), \alpha_2(t) = 0; \phi_1(t) = \phi(t), \phi_2(t) = 0. \tag{II.11}$$

Also, for algebraic tractability, we have found it necessary to assume

$$\sigma_2(t) = \sigma_1(t) \equiv \sigma(t). \tag{II.12}$$

While this ties the widths of the $A(x, t)$ and $r(x, t)$ fields together, the loss of generality is acceptable since the field $r(x, t)$ has no real physical significance. Moreover, for the snaking soliton solutions, we choose $\sigma(t) = 2/\phi(t)$. By using all these assumptions, the trial functions (II.8)-(II.9) become

$$A(x, t) = A_1(t) e^{-\frac{4}{\phi(t)^2} [x - \phi(t)]^2} e^{i\alpha(t)} \tag{II.13}$$

$$r(x, t) = e^{-\frac{4}{\phi(t)^2} x^2}. \tag{II.14}$$

Substituting the last two equations into (II.10), the effective Lagrangian becomes

$$\begin{aligned}
L_{EFF} = \frac{\sqrt{\pi}}{12e^{\frac{10}{3}} \phi(t)} \left[& 6e^{\frac{1}{3}} A_1(t)^3 \phi(t)^2 (b_3 \cos \alpha(t) + c_3 \sin \alpha(t)) \right. \\
& + 2\sqrt{6} A_1(t)^5 \phi(t)^2 (b_5 \cos \alpha(t) + c_5 \sin \alpha(t)) \\
& - 3\sqrt{2} e^{-\frac{4}{3}} \left(-2A_1(t) \sin \alpha(t) (-12c_1 + \phi(t)^2 \dot{\alpha}(t)) \right. \\
& \left. \left. \left. + \cos \alpha(t) (-2\phi^2(t) \dot{\alpha}(t) + A_1(t)(24b_1 + 2\epsilon\phi^2(t) + 3\phi(t)\dot{\phi}(t))) \right) \right) \right]. \tag{II.15}
\end{aligned}$$

We are left with three parameters $A_1(t)$, $\phi(t)$ and $\alpha(t)$ in L_{EFF} . Varying these parameters by using calculus of variations, we obtain

$$\frac{\partial L_{EFF}}{\partial \star(t)} - \frac{d}{dt} \left(\frac{\partial L_{EFF}}{\partial \dot{\star}(t)} \right) = 0, \quad (\text{II.16})$$

where \star refers to A_1 , α , or ϕ . Solving for $\dot{\star}(t)$, we obtain the following system of three ordinary differential equations,

$$\begin{aligned} \dot{A}_1(t) &= f_1[A_1(t), \alpha(t), \phi(t)] \\ \dot{\alpha}(t) &= f_2[A_1(t), \alpha(t), \phi(t)] \\ \dot{\phi}(t) &= f_3[A_1(t), \alpha(t), \phi(t)] \end{aligned} \quad (\text{II.17})$$

where the right hand side f_1, f_2, f_3 of (II.17) are given by

$$\begin{aligned} f_1 &= \frac{1}{5} A_1(t) \sec \alpha(t) (3456 c_1 e^{8/3} \sin \alpha(t) (-b_1 \cos \alpha(t) + c_1 \sin \alpha(t)) \\ &\quad + A_1(t)^2 \phi(t)^2 (2\sqrt{6} e^{1/3} A_1(t)^4 (5b_3 b_5 + 17c_3 c_5 + (3b_3 b_5 - 19c_3 c_5) \cos(2\alpha(t))) \\ &\quad + (-2b_3 b_5 + 2c_3 c_5) \cos(4\alpha(t)) + (b_5 c_3 + b_3 c_5) (11 \sin(2\alpha(t)) - 2 \sin(4\alpha(t)))) \phi(t)^2 \\ &\quad + 4A_1(t)^6 (4b_5^2 + 13c_5^2 + (2b_5^2 - 15c_5^2) \cos(2\alpha(t)) + 2(-b_5^2 + c_5^2) \cos(4\alpha(t))) \\ &\quad + 17b_5 c_5 \sin(2\alpha(t)) - 4b_5 c_5 \sin(4\alpha(t))) \phi(t)^2 + 3e^{2/3} A_1(t)^2 (3b_3^2 + 11c_3^2 \\ &\quad + 2(b_3^2 - 6c_3^2) \cos(2\alpha(t)) + (-b_3^2 + c_3^2) \cos(4\alpha(t)) - 2b_3 c_3 (-7 \sin(2\alpha(t)) \\ &\quad + \sin(4\alpha(t)))) \phi(t)^2 + 6\sqrt{2} e^{5/3} (6b_1 b_3 - 18c_1 c_3 + 6(b_1 b_3 + c_1 c_3) (2 \cos(2\alpha(t)) \\ &\quad + \cos(4\alpha(t))) - 48(b_3 c_1 - b_1 c_3) \cos \alpha(t)^3 \sin \alpha(t) - 2\epsilon \cos \alpha(t) (b_3 \cos \alpha(t) \\ &\quad + 3c_3 \sin \alpha(t)) \phi(t)^2) + 4\sqrt{3} e^{4/3} A_1(t)^2 (12b_1 b_5 - 36c_1 c_5 \\ &\quad + 12(b_1 b_5 + c_1 c_5) (2 \cos(2\alpha(t)) + \cos(4\alpha(t))) - 96(b_5 c_1 - b_1 c_5) \cos \alpha(t)^3 \sin \alpha(t) \\ &\quad - 2\epsilon \cos \alpha(t) (2b_5 \cos \alpha(t) + 5c_5 \sin \alpha(t)) \phi(t)^2)) e^{-4/3} / \phi(t)^2 / (144c_1 e^{4/3} \sin \alpha(t) \\ &\quad + A_1(t)^2 (-3\sqrt{2} e^{1/3} (-3b_3 \cos \alpha(t) + b_3 \cos(3\alpha(t)) - 11c_3 \sin \alpha(t) + c_3 \sin(3\alpha(t))) \\ &\quad + 4\sqrt{3} A_1(t)^2 (4b_5 \cos \alpha(t) - 2b_5 \cos(3\alpha(t)) + 13c_5 \sin \alpha(t) \\ &\quad - 2c_5 \sin(3\alpha(t)))) \phi(t)^2) \end{aligned} \quad (\text{II.18})$$

$$\begin{aligned} f_2 &= \frac{1}{15} (-72e^{4/3} (b_1 - c_1 \tan \alpha(t)) + (-6e^{4/3} \epsilon + 9\sqrt{2} e^{1/3} A_1(t)^2 (b_3 + c_3 \tan \alpha(t)) \\ &\quad + 10\sqrt{3} A_1(t)^4 (b_5 + c_5 \tan \alpha(t))) \phi(t)^2 e^{-4/3} / \phi(t) \end{aligned} \quad (\text{II.19})$$

$$\begin{aligned} f_3 &= \frac{2}{5} (-144c_1 e^{7/3} \epsilon \cos \alpha(t) - \sqrt{6} A_1(t)^6 ((b_5 c_3 - 3b_3 c_5) \cos \alpha(t) \\ &\quad + (b_5 c_3 + b_3 c_5) \cos(3\alpha(t)) - 2(b_3 b_5 + c_3 c_5 + (b_3 b_5 - c_3 c_5) \cos(2\alpha(t))) \sin \alpha(t)) \phi(t)^2 \\ &\quad + 6\sqrt{2} e^{4/3} A_1(t)^2 (12(b_3 c_1 + 3b_1 c_3) \cos \alpha(t) + 12(b_3 c_1 - b_1 c_3) \cos(3\alpha(t)) \\ &\quad + 12(b_1 b_3 - 3c_1 c_3) \sin \alpha(t) + 12(b_1 b_3 + c_1 c_3) \sin(3\alpha(t)) + \epsilon \cos \alpha(t) (c_3 (-2 \\ &\quad + \cos(2\alpha(t))) - b_3 \sin(2\alpha(t))) \phi(t)^2) + 8\sqrt{3} e A_1(t)^4 (36b_1 c_5 \cos \alpha(t) \\ &\quad + 18(b_5 c_1 - b_1 c_5) \cos(3\alpha(t)) + 18(b_1 b_5 - 3c_1 c_5) \sin \alpha(t) + 18(b_1 b_5 + c_1 c_5) \sin(3\alpha(t)) \\ &\quad + \epsilon \cos \alpha(t) (-3c_5 + 2c_5 \cos(2\alpha(t)) - 2b_5 \sin(2\alpha(t))) \phi(t)^2)) e^{-1} / (144c_1 e^{4/3} \sin \alpha(t) \\ &\quad + A_1(t)^2 (-4\sqrt{2} e^{1/3} (-3b_3 \cos \alpha(t) + b_3 \cos(3\alpha(t)) - 11c_3 \sin \alpha(t) \\ &\quad + c_3 \sin(3\alpha(t))) + 4\sqrt{3} A_1(t)^2 (4b_5 \cos \alpha(t) - 2b_5 \cos(3\alpha(t)) + 13c_5 \sin \alpha(t) \\ &\quad - 2c_5 \sin(3\alpha(t)))) \phi(t)^2) \end{aligned} \quad (\text{II.20})$$

The Euler-Lagrange equations (II.17) are treated in a completely novel way. Rather than considering the stable fixed points which correspond to the well-known stationary solitons or plain pulses, we use Hopf bifurcation theory to focus on periodic attractors. Periodic evolution of the trial function parameters on stable periodic attractors yields the pulsating soliton whose amplitude is non-stationary or time dependent.

We derive the conditions for the temporal Hopf bifurcations of the fixed points. The conditions for supercritical temporal Hopf bifurcations, leading to stable periodic orbits of $A_1(t)$, $\phi(t)$, and $\alpha(t)$ can be evaluated using the method of Multiple Scales, as in [11]. These are the conditions or parameter regimes which exhibit stable periodic oscillations, and hence stable pulsating solitons will exist within our variational formulation. Note that, it is easy to verify numerically, periodic oscillations of $A_1(t)$, $\phi(t)$, and $\alpha(t)$, correspond to a spatiotemporal pulsating soliton structure of the $|A(x, t)|$ given by (II.8).

The fixed points of (II.17) are given by a complicated system of transcendental equations. These are solved numerically to obtain results for each particular case.

For a typical fixed point, the characteristic polynomial of the Jacobian matrix of a fixed point of (II.17) may be expressed as

$$\lambda^3 + \delta_1 \lambda^2 + \delta_2 \lambda + \delta_3 = 0 \tag{II.21}$$

where δ_i with $i = 1...3$ depend on the system parameters and the fixed points. Since these are extremely involved, we omit the actual expressions, and evaluate them numerically where needed.

To be a stable fixed point within the linearized analysis, all the eigenvalues must have negative real parts. Using the Routh-Hurwitz criterion, the necessary and sufficient conditions for (II.21) to have $Re(\lambda_{1,2,3}) < 0$ are:

$$\delta_1 > 0, \quad \delta_3 > 0, \quad \delta_1 \delta_2 - \delta_3 > 0. \tag{II.22}$$

On the contrary, one may have the onset of instability of the plane wave solution occurring in one of the two ways. In the first, one root of (II.17) (or one eigenvalue of the Jacobian) becomes non-hyperbolic by going through zero for

$$\delta_3 = 0. \tag{II.23}$$

Equation (II.23) is thus the condition for the onset of “static” instability of the plane wave. Whether this bifurcation is a pitchfork or transcritical one, and its subcritical or supercritical nature, may be readily determined by deriving an appropriate canonical system in the vicinity of (II.23) using any of a variety of normal form or perturbation methods.

One may also have the onset of dynamic instability (“flutter” in the language of Applied Mechanics) when a pair of eigenvalues of the Jacobian become purely imaginary. The consequent Hopf bifurcation at

$$\delta_1 \delta_2 - \delta_3 = 0 \tag{II.24}$$

leads to the onset of periodic solutions of (II.17) (dynamic instability or ”flutter”).

III. NUMERICAL METHODS

A. The Initial Boundary Value Problem of the CCQGLE

To obtain the snaking soliton solutions that are periodic and exponentially decaying at infinity, we develop numerical schemes for the IBVP of (II.1) with $A(a, \cdot) = A(b, \cdot)$, and $A(0, \cdot) = A_0(\cdot)$ based on the finite difference method as described below.

Let $h = (b - a)/n$ be the grid spacing and $x_j = a + jh, j = 0, 1, \dots, n$ be the grid points. Define $A_j(t)$ as an approximation to $A(x_j, t), j = 0, 1, \dots, n$, $\mathbf{A}(t) = (A_1(t), \dots, A_{n-1}(t))^T$ and $\mathbf{A}_0(x) = (A_0(x_1), \dots, A_0(x_{n-1}))^T$. Let $F(A_j(t)) = \epsilon A_j(t) - (b_3 - ic_3)|A_j(t)|^2 A_j(t) - (b_5 - ic_5)|A_j(t)|^4 A_j(t)$. Using the central difference approximation to $\partial_x^2 A(x_j, t)$, we write the semi-discretization of the IBVP of (II.1) as

$$\dot{\mathbf{A}}(t) = \mathcal{B}\mathbf{A}(t) + \mathbf{F}(\mathbf{A}(t)), \forall t > 0, \quad (\text{III.1})$$

$$\mathbf{A}(0) = \mathbf{A}_0, \quad (\text{III.2})$$

where $\mathbf{F}(\mathbf{A}(t)) = (F(A_1(t)), \dots, F(A_n(t)))^T$. The upper dot in (III.1) indicates derivative with respect to t and \mathcal{B} is the finite difference matrix. To construct an integration scheme to solve the ODE system (III.1)-(III.2), let $t_{n+1} = t_n + \Delta t$, and let \mathbf{A}^n denote the value of the variable \mathbf{A} at time t_n . Employing a low storage variant third-order Runge-Kutta scheme [14], we write the fully discrete system as

$$\begin{aligned} \mathbf{Q}_1 &= \Delta t \mathbf{G}(\mathbf{A}^n), & \mathbf{A}_1 &= \mathbf{A}^n + \frac{1}{3} \mathbf{Q}_1, \\ \mathbf{Q}_2 &= \Delta t \mathbf{G}(\mathbf{A}_1) - \frac{5}{9} \mathbf{Q}_1, & \mathbf{A}_2 &= \mathbf{A}_1 + \frac{15}{16} \mathbf{Q}_2, \\ \mathbf{Q}_3 &= \Delta t \mathbf{G}(\mathbf{A}_2) - \frac{153}{128} \mathbf{Q}_2, & \mathbf{A}^{n+1} &= \mathbf{A}_2 + \frac{8}{15} \mathbf{Q}_3, \end{aligned} \quad (\text{III.3})$$

where $\mathbf{G}(\mathbf{A}^n) = \mathcal{B}\mathbf{A}^n + \mathbf{F}(\mathbf{A}^n)$. The numerical code is parallelized for distributed memory clusters of processors or heterogeneous networked computers using the MPI (Message Passing Interface) library and implemented in FORTRAN.

Computations were performed on a Linux cluster (zeus.db.erau.edu: 256 Intel Xeon 3.2GHz 1024 KB cache 4GB with Myrinet MX, GNU Linux) at Embry-Riddle Aeronautical University.

B. The Initial Value Problem of Euler-Lagrange System

The system of ODEs (II.17) resulting from the variational approximation to the PDE is solved numerically using the MATLAB's built-in function `ode45` (adaptive fourth- and fifth-order Runge-Kutta-Fehlberg method). We use equilibrium solution $A_1(0) = A_1^0$, $\alpha(0) = \alpha^0$, $\phi(0) = \phi^0$ of the system (II.17) as the initial conditions. The numerical solutions A_1^n , α^n , ϕ^n giving the approximations to $A_1(t_n)$, $\alpha(t_n)$, $\phi(t_n)$ are used to evaluate $A(x_j, t_n)$, approximation to the snaking soliton solution to the CCQGLE, in the spatial grids x_j at time t_n using the following formula

$$A(x_j, t_n) = A_1^n e^{-\sigma^2(x_j - \phi^n)^2} e^{i\alpha^n},$$

where $\sigma = 2/\phi^n$.

IV. RESULTS AND DISCUSSION

A. Simulations of Snake Solitons using the PDE

The numerical scheme for the PDE described in section §3 is implemented with the following initial amplitude profile

$$A(x, 0) = A_1 e^{-\sigma^2(x - \phi)^2} e^{i\alpha}. \quad (\text{IV.1})$$

We use $A_1 = 0.583236$, $\phi = 1.05969$, $\alpha = 0.185515$ and $\sigma = 1.8873$ as the typical values of the parameters in (IV.1). These are the values of the fixed point as we will see in the next section. For the system parameters of the PDE (II.1), initially we use the values listed in Table 1 (see the row for snaking soliton). In [9] five novel classes of dissipative soliton solutions viz. pulsating, creeping, snaking, exploding and chaotic were obtained by numerical simulations of the CCQGLE (II.1). Here we present a theoretical formulation to one class of the solutions, the snake, we perform independent simulations on the full PDE from the ones shown previously in [1], and we also compare the result with the simulations from the variational approximation. First, for the simulations on the PDE, we fix a set of system parameters ϵ , b_1 , b_3 , b_5 , c_1 , c_3 , c_5 for the snake soliton from the Table 1. Then, we study the qualitative behavior of the snaking soliton by varying one parameter at a time. Then, we present the spatio-temporal structure of the snaking soliton in detail using the numerical simulations of the variational approximation to CCQGLE in the next section. The spatio-temporal structure of the solitons obtained from the simulations of the partial differential equation (CCQGLE) is shown in Figs. 1-4. In each of the solitons presented in Figs. 1-4 one of the parameters is

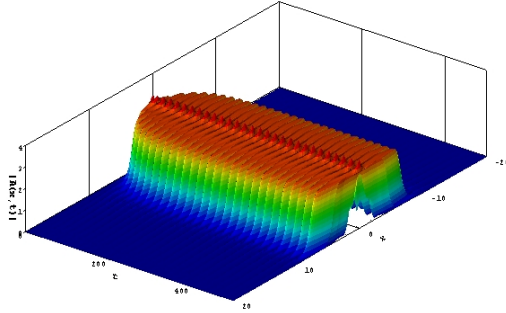


FIG. 1: Numerical simulation of snaking soliton using the PDE: unperturbed case

TABLE I: Parameters of the CCQGLE

Solitons	ϵ	b_1	c_1	b_3	c_3	b_5	c_5
Pulsating	-0.1	0.080	0.5	-0.660	1	0.10	-0.100
Creeping	-0.1	0.101	0.5	-1.300	1	0.30	-0.101
Snaking	-0.1	0.080	0.5	-0.835	1	0.11	-0.080
Exploding	-0.1	0.125	0.5	-1.000	1	0.10	-0.600
Chaotical	-0.1	0.125	0.5	-0.300	1	0.10	-1.000

perturbed while all the other remaining parameters are chosen from the Table 1 (see the row for the snake soliton, which is the unperturbed case). Thus, only the perturbed parameter is indicated in the captions to the figures while the other ones stay unchanged.

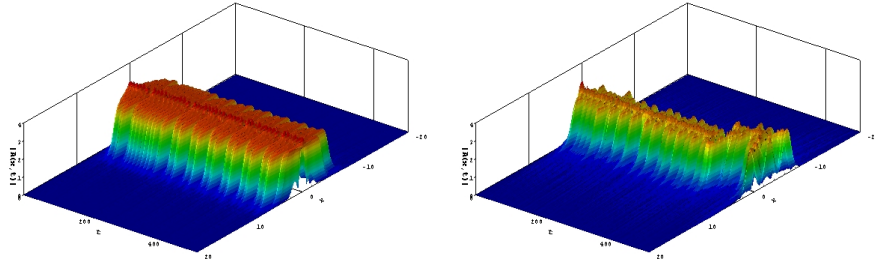


FIG. 2: Perturbed snaking soliton using the PDE: Left $b_3 = -0.8$, Right $b_5 = 0.15$

V. SNAKE SOLITONS USING VARIATIONAL APPROXIMATION

In our previous work [10], we looked at stationary soliton solutions of the CCQGLE in the parameter regimes where they exist. However, these are not the only possible type of solutions. Pulsating solutions are another example of localized structures. They arise naturally from the stationary ones when the latter become unstable. Pulsating solitons might have several frequencies in their motions and the solutions will be quasiperiodic. A relative simpler case is when the motion has two frequencies. Then, we will have a pulsating soliton [11], which instead of having a zero velocity will move back and forward around a fixed point. Obviously, there are two frequencies involved in this motion which usually are incommensurate. We call this type of solitons with more than one frequency a snaking soliton. To capture this, we will use dynamical systems theory to construct solitons with quasiperiodic behavior.

Stable fixed points of the Euler-Lagrange system (II.17) corresponds to the well-known stationary solitons or plain pulses. The periodic evolution of $A_1(t)$, $\phi(t)$, $\alpha(t)$ on stable periodic attractors yields solitons whose

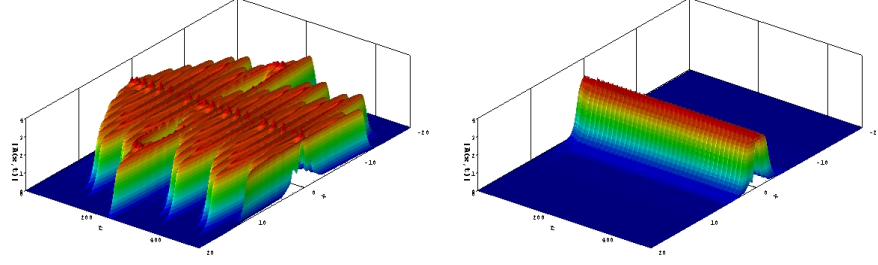


FIG. 3: Perturbed snaking soliton using the PDE: Left $c_1 = 0.55$, Right $c_3 = 1.135$

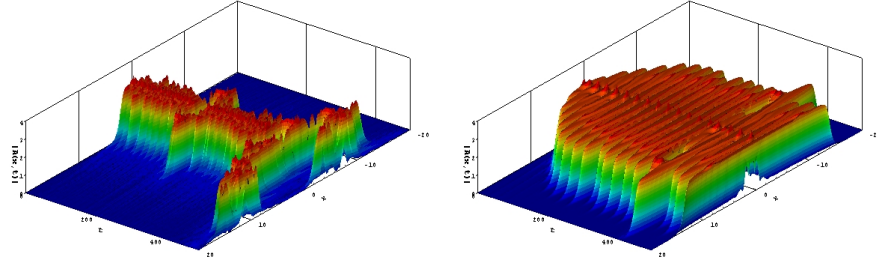


FIG. 4: Perturbed snaking soliton using the PDE: Left $c_5 = -0.06$, Right $\epsilon = -0.08$

amplitude is non-stationary. To derive the conditions for occurrence of stable periodic orbits of $A_1(t)$, $\phi(t)$, and $\alpha(t)$, we proceed as follows.

First, we fix a set of system parameters $b_1 = 0.08$, $b_5 = 0.11$, $c_1 = 0.5$, $c_3 = 1$, $c_5 = -0.08$ as in the case of the full PDE presented in the Table 1. Then, we solve numerically the system of transcendental equations (II.17), which are the equations of the fixed points. By the Ruth-Hurwitz conditions, the Hopf curve is defined as $\delta_1\delta_2 - \delta_3 = 0$. This condition, along with the equations of the fixed points leads to onset of periodic solutions of (II.17) as we will see next. On the Hopf bifurcation curve we obtain that

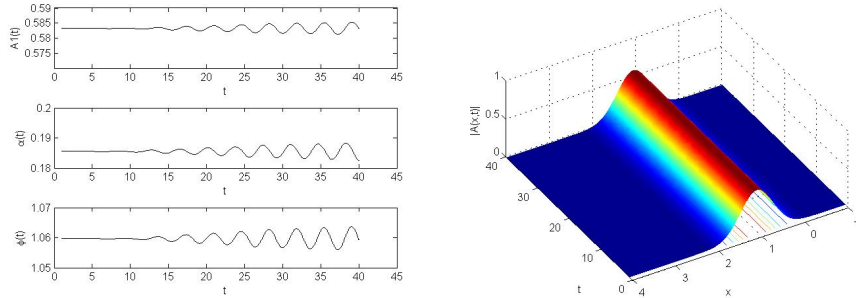


FIG. 5: Numerical simulation using the variational approximation: periodic time series of the amplitude $A_1(t)$, the phase $\alpha(t)$ and the position $\phi(t)$ on the Hopf curve (Left), spatiotemporal structure of the amplitude $|A(x,t)| = A_1^n e^{-\sigma^2(x_j - \phi^n)^2}$ on the Hopf curve (Right).

$b_{3Hopf} = -1.89646$, and $\epsilon_{Hopf} = -0.297393$, while the fixed points are $A_1(0) = 0.583236$, $\phi(0) = 1.05969$, and $\alpha(0) = 0.185515$. For these values of b_{3Hopf} and ϵ_{Hopf} , which are two free bifurcation parameters, we integrate numerically the systems of 3 ODEs (II.17), using as initial conditions the three values of the fixed points, to find the trial function's periodic functions. Hopf bifurcations occur in this system leading to periodic orbits. These are the conditions which exhibit periodic oscillations, and hence stable snaking solitons will exist within our variational formulation.

Next, we plot the time series for the amplitude $A_1(t)$, the phase $\alpha(t)$ and the position $\phi(t)$ on the Hopf curve and the results are presented in Fig. 5 (Left). As expected, we noticed that the amplitude is small, since the maximum height of the snaking soliton is proportional to the square root of the distance from the Hopf curve. The corresponding spatio-temporal structure of the ansatz $|A(x, t)| = A_1^n e^{-\sigma^2(x_j - \phi^n)^2}$ on the Hopf curve is shown in Fig. 5 (Right). Notice in the figure very small undulations in amplitude.

To construct snake solitons with amplitudes large enough, we had to move away from the Hopf curve, as much as possible, but at the same time to be sure not to be outside of the parameters ranges for the existence of the snaking soliton. That could be achieved by varying one or more of the system parameters. First, we varied the first bifurcation parameter ϵ , slowly away from the Hopf curve where $b_3 = b_{3Hopf}$, and $\epsilon = \epsilon_{Hopf}$, and we noticed that the snaking soliton had very small amplitude of $A_1(t)$. Since the soliton in this case had only a magnitude of only 10^{-4} , we decided to vary the second bifurcation parameter b_3 , which stands for the cubic gain when negative. We found that the domain of existence for the snaking soliton as a function of b_3 was $[-2.25234, -0.143456]$, passing through the Hopf curve value of $b_{3Hopf} = -1.89646$. For the unperturbed values of $b_3 = -0.835$, and $\epsilon = -0.1$, we numerically integrate the Euler-Lagrange system of ODEs (II.17) using the Matlab's built-in function `ode45` and we plot the periodic orbit, which is shown in Fig. 6 (Left), while the resulting periodic time series for $A_1(t)$, $\alpha(t)$, and $\phi(t)$ are shown in Fig. 6 (Right). The resulting time series are then substituted back in the ansatz (II.13) and the spatiotemporal structure $|A(x, t)|$ of the snaking soliton obtained by the variational formulation is presented in Fig. 7. As the various system parameters $c_1, c_3, c_5, b_1, b_3, b_5$, and ϵ within the stable regime are varied, the effects of the amplitude, position, width (and, less importantly, phase) may also be studied, and this is discussed subsequently. As

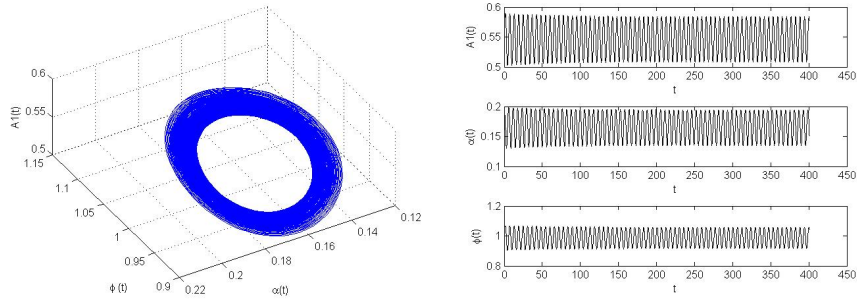


FIG. 6: Numerical simulation using the variational approximation for the snake of Fig. 1: periodic orbit or limit cycle (Left), periodic time series for $A_1(t)$, $\alpha(t)$, and $\phi(t)$ (Right)

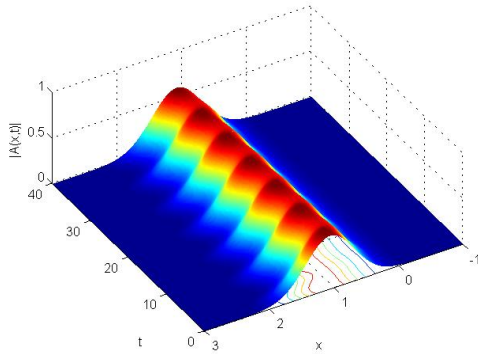


FIG. 7: Snake soliton using the ODEs (variational approximation): unperturbed case

observed from the simulations of the full PDE and ODEs system, the snaking soliton obtained from the ODE system (II.17) qualitatively agree for a short time to the solution of the complex nonlinear PDE (II.1). Let us take a closer look to the snake solitons shown in Figs. 7–10. The soliton now “snakes” or wiggles as

its position varies periodically in time. Note that the amplitude $|A(t)|$ varies periodically as $A_1(t)$ varies¹¹, but there would be additional amplitude modulation due to the periodic variation of $\phi(t)$. Next, we shall consider the effect of all the various parameters in the CCQGLE (II.1) on the shape (amplitude, position, phase, period) and stability of the snake.

In considering the parameter effects on snake shape and period, note that the wave is a spatially coherent structure (or a “collective coordinate” given by the trial function) whose parameters oscillate in time. Hence, the temporal period of the snake is the same as the period T of the oscillations of $A_1(t)$, $\phi(t)$, and $\alpha(t)$ on their limit cycle. As for the peak amplitude and peak position of the snake, these are determined by the peak amplitude A_{1p} of $A_1(t)$, and the peak position ϕ_p of $\phi(t)$ respectively. Notice that from (II.13) we can regard the width and the amplitude of the snake as being inversely proportional to position $\phi(t)$ for the snake i.e., at any time t when the amplitude is minimum, the width will be minimum, so the position is maximum and vice versa. So, maximum deflection from the horizontal position $x = \text{const.}$ is obtained when the position of the snake is maximum, and hence the width and amplitude are minimum.

Keeping the above in mind, we vary the parameters of the CCQGLE in turn and we observe the resulting effects on A_{1p} (the peak amplitude), ϕ_p (the position), and T (the temporal period) of the snake soliton:

- (i) For *increased* b_1 , the values of A_{1p} , ϕ_p , and T all *increase*.
- (ii) *Increasing* b_3 *augments* all of A_{1p} , ϕ_p , and T .
- (iii) *Increasing* b_5 *increases* all of A_{1p} , ϕ_p , and T .
- (iv) *Raising* c_1 *increases* A_{1p} , ϕ_p , but *decreases* T .
- (v) *Incrementing* c_3 *decreases* all of A_{1p} , ϕ_p , and T .
- (vi) *Augmenting* c_5 causes a *decrease* in A_{1p} , ϕ_p , and *increases* T .
- (vii) *Raising* ϵ causes A_{1p} , σ_p to *rise*, but T to *fall*.

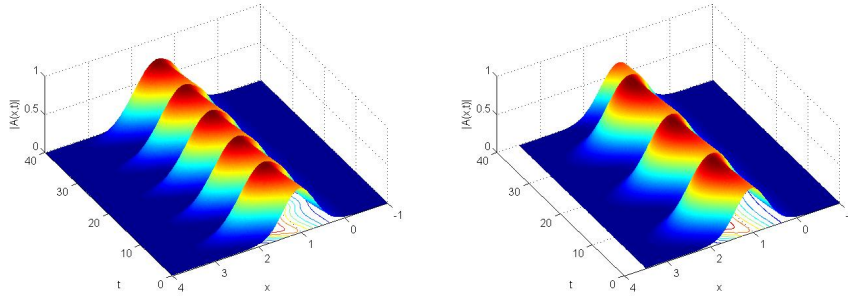


FIG. 8: Snake soliton using the ODEs (variational approximation): Left $b_3 = -0.6$, Right $b_3 = 0.62$

The above constitute our detailed predictions of the various parameters in the CCQGLE on the amplitude, position, and temporal width of the snake solitons. We have verified that each set of predictions (i)-(vii) above agree when the corresponding parameter is varied in the solitary wave simulation for the full PDE. Note also that $A_1(t)$ and $\phi(t)$ are always in phase, so that A_{1p} and ϕ_p occur simultaneously. Thus, the snaking solitons are tallest where they have the greatest width. This is completely consistent with our simulation, as well as those in [3].

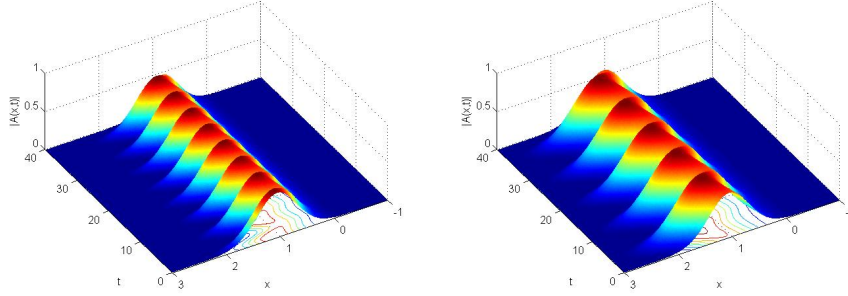


FIG. 9: Snake soliton using the ODEs (variational approximation): Left $c_1 = 0.55$, Right $c_3 = 2$

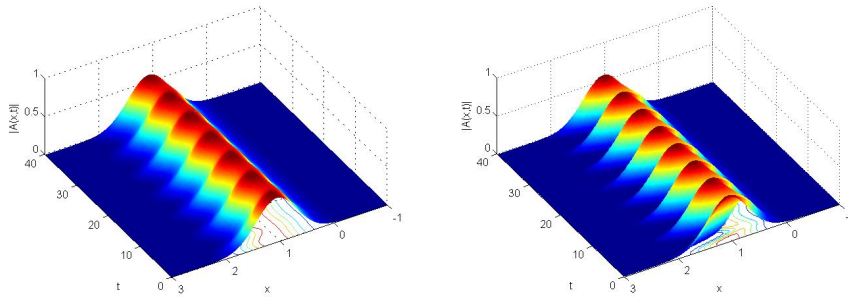


FIG. 10: Snake soliton using the ODEs (variational approximation): Left $c_5 = 0.8$, Right $\epsilon = -0.08$

VI. CONCLUSION

In this paper we discussed a brief theoretical framework for analyzing the full spatiotemporal structure of one class of solitary waves (snaking soliton) in the CCQGLE and presented some numerical simulations of dissipative snaking soliton solutions to the CCQGLE. The results obtained analytically using the variational approximation for the snaking soliton is compared with the numerical simulations of the CCQGLE. The specific theoretical modeling includes the use of a recent variational formulation and significantly generalized trial function for the solitary waves solutions. In addition, the resulting Euler-Lagrange equations are treated in an entirely different way by looking at their stable periodic solutions (or limit cycles) resulting from supercritical Hopf bifurcations. Oscillations of their trial function parameters on these limit cycles provide the pulsations of the amplitude, width/position, and phase of the solitons. The model also allows for detailed predictions regarding the other types of solitons i.e., pulsating, chaotic and creeping.

In the future, we will explore on the (2D) solutions called spinning solitons as well as the (3D) solutions called optical bullets. These depict a confined spatiotemporal soliton in which the balance between the focusing nonlinearity and the spreading while propagating through medium provides the shape of a bullet [5, 12].

-
- [1] N. Akhmediev, J. M. Soto-Crespo, and G. Town. Pulsating solitons, chaotic solitons, period doubling, and pulse coexistence in mode-locked laser: CGLE approach. *Phys. Rev.E*, 63:56602, 2001.
 - [2] I.S. Aranson and L.Kramer. The world of the Complex Ginzburg-Landau equation. *Rev. Mod. Phys.*, 74:99, 2002.
 - [3] D. Artigas, L. Torner, and N. Akhmediev. Robust heteroclinic cycles in the one-dimension CGLE. *Opt. Comm.*, 143:322, 1997.
 - [4] F. Cariello and M. Tabor. Painlevé expansions for non-integrable evolution equations. *Physica D*, 39:77, 1989.

- [5] L. Crasovan, B. Malomed, and D. Mihalache. Spinning solitons in cubic–quintic nonlinear media. *Pramana J.Phys.*, 57:1041, 2001.
- [6] S. Fauve and O. Thual. Solitary waves generated by subcritical instabilities in dissipative systems. *Phys. Rev. Lett.*, 64:282, 1990.
- [7] N. Akhmediev K. Maruno, A. Ankiewicz. Exact soliton solutions of the one–dimensional complex Swift–Hohenberg equation. *Physica D*, 176:44, 2003.
- [8] D.J. Kaup and B.A. Malomed. The variational principle for nonlinear waves in dissipative systems. *Physica D*, 87:155, 1995.
- [9] H. Khanal and S. Mancas. Numerical Simulations of Five Novel Classes of Dissipative Solitons. *Proceedings of the 2008 International Conference on Computational and Mathematical Methods in Science and Engineering*, 2:354, 2008.
- [10] S.C. Mancas. *Dissipative solitons in the cubic–quintic complex Ginzburg–Landau equation: bifurcations and spatiotemporal structure*. PhD thesis, University of Central Florida, 2007.
- [11] S.C. Mancas and S. R. Choudhury. A novel variational approach to pulsating solitons in the cubic–quintic Ginzburg–Landau equation. *Teoreticheskaya i Matematicheskaya Fizika*, 152:339, 2007.
- [12] J.M. Soto-Crespo, N. Akhmediev, and P. Grelu. Optical bullets and double bullet complexes in dissipative systems. *Phys.Rev.E*, 74:046612, 2006.
- [13] W. van Saarloos and P.C. Hohenberg. Fronts, pulses, sources and sinks in generalized complex Ginzburg–Landau equation. *Phys.D*, 56:303, 1992.
- [14] J. Williamson. Low-storage Runge-Kutta schemes. *J. Comp. Phys.*, 35:48, 1980.